Generation of Porous Structures Using Fused Deposition

Bertoldi M., Yardimci M. A., Pistor C. M., Güçeri S. I., Danforth S. C.
University of Illinois at Chicago & Rutgers University

ABSTRACT

The Fused Deposition Modeling process uses hardware and software machine-level language that are very similar to that of a pen-plotter. Consequently, the use of patterns with poly-lines as basic geometric features, instead of the current method based on filled polygons (monolithic models), can increase its efficiency.

In the current study, various toolpath planning methods have been developed to fabricate porous structures. Computational domain decomposition methods can be applied to the physical or to slice-level domains to generate structured and unstructured grids. Also, textures can be created using periodic tiling of the layer with unit cells (squares, honeycombs, etc). Methods based on curves include fractal space filling curves and change of effective road width within a layer or within a continuous curve. Individual phases can also be placed in binary compositions.

In present investigation, a custom software has been developed and implemented to generate build files (SML) and slice files (SSL) for the above-mentioned structures, demonstrating the efficient control of the size, shape, and distribution of porosity.

INTRODUCTION

Two dimensional pattern generation capability of RP/SFF methods is not being fully utilized currently due to use of very limited set of toolpath generation algorithms and data representation problems associated with heterogeneous structures. Generation of controlled porosity structures with RP/SFF has been particularly challenging due to the need of defining the entire porous structure as a very complicated solid object.

Porosity generation within solid models with RP/SFF processes has been investigated in the context of investment casting with SLA fabricated constant pore size patterns. Two-dimensional equilateral triangular and square self-repeating patterns were developed by 3D Systems, three-dimensional laminated hexagonal structures by the University of Nottingham group [1] and three-dimensional tetragonal crystalline structures by Gervasi and coworkers [2].

Recently, rectangular porous interior structures were adopted by Stratasys in Fused Deposition and tetragonal patterns by Z-Corporation in 3D printing for build acceleration. The computational geometry definition problem of heterogeneous structures has been investigated [3]; however, this study does not address the generation of porous structures inside solid models.

Fused Deposition can be considered as a vector printing technique, in which the two-dimensional patterns are generated with poly-lines on a discretized *x-y* plane. Boundary deposition and subsequent raster filling is employed during production; voids appear in the raster filling, due to the finite road width; this can be used to produce specific porosity. However, current Fused Deposition process planning software only allows for constant layer thickness across the entire part, constant road width within each layer, contour or rectilinear rasters, monolithic material composition, and constant air-gap between raster patterns. As a result, the variety of attainable porous structures is very limited.

A set of software tools has been developed and used to generate porous structures, showing the feasibility of the concepts presented. Since layer geometries are inherently two-dimensional, the remainder of the presentation will be focused on two-dimensional grid generation.

TWO DIMENSIONAL TEXTURES

Basic texture structures employed by computer graphics methods, such as square blocks and honeycombs, can fill a plane by tiling the basic unit periodically. The variety of micro-structures can be increased by recursively constructing higher-order unit cells that fill the plane through periodic tiling, as shown in Figure 1.

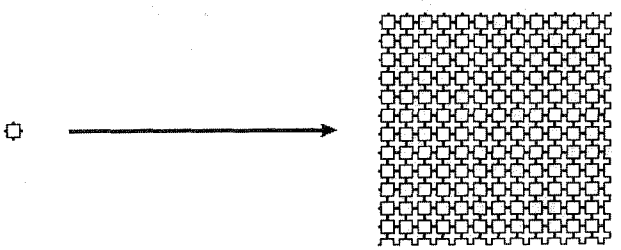

Figure 1 *Unit cell and resulting texture.*

Texture based patterns can be generated once the underlying unit cell is designed properly to fill the entire plane. The texture needs to be clipped to fit into the layer geometry described by the contours, which increases the computational requirements. The unit cell nature of the textures enforces a homogeneous pore size and microstructure distributions throughout the entire part, which limits the use of this technique.

STRUCTURED GRID GENERATION

Structured grids are used in the simulation of complex physical processes, where discretization of the domain of interest into geometrically simple sub-structures is required. Systems of algebraic or ordinary differential equations representing the physical phenomena are defined over the discretized domain, with appropriate variable transformations [4]. Uniform Cartesian grids within rectangles and circular geometries can be generated, employing linear functions and coordinate transformations, as depicted in Figure 2.

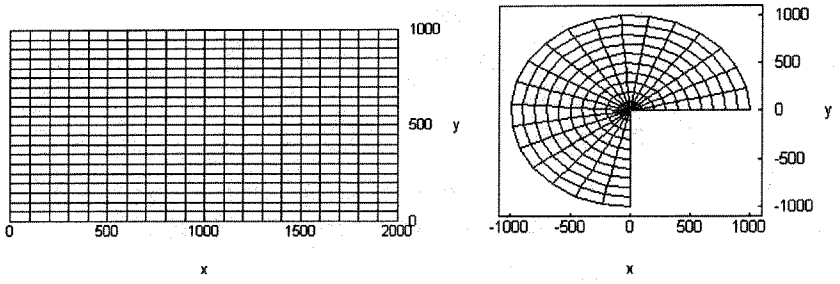

Figure 2 *Uniform Cartesian grids.*

The resultant grids have regular porosity distributions, which can be manipulated only by varying grid spacing independently along the coordinate axes. The porosity can be better controlled through use of nonlinear stretching functions as mapping functions from computational to physical space. One example of stretching functions to generate boundary clustering is:

$$\begin{Bmatrix} x \\ y \end{Bmatrix} = \begin{Bmatrix} (x_{\max} - x_{\min}) \dfrac{(2\alpha+\beta)\left[(\beta+1)/(\beta-1)\right]^{(\xi-\alpha)/(1-\alpha)} + 2\alpha - \beta}{(2\alpha+1)\left\{1+\left[(\beta+1)/(\beta-1)\right]^{(\xi-\alpha)/(1-\alpha)}\right\}} + x_{\min} \\ (y_{\max} - y_{\min}) \dfrac{(2\alpha+\beta)\left[(\beta+1)/(\beta-1)\right]^{(\eta-\alpha)/(1-\alpha)} + 2\alpha - \beta}{(2\alpha+1)\left\{1+\left[(\beta+1)/(\beta-1)\right]^{(\eta-\alpha)/(1-\alpha)}\right\}} + y_{\min} \end{Bmatrix} \quad (1)$$

where ξ and η denote coordinates in computational space. The generated grids are presented in Figure 3.

Although Cartesian grids are powerful geometric discretization tools for simple domains, they are not directly adaptable for arbitrary two-dimensional domains and have to be used as background textures with polygon clipping methods. Complex geometry physical simulation

necessitated the development of boundary conforming, or boundary fitted curvilinear grid methods [5].

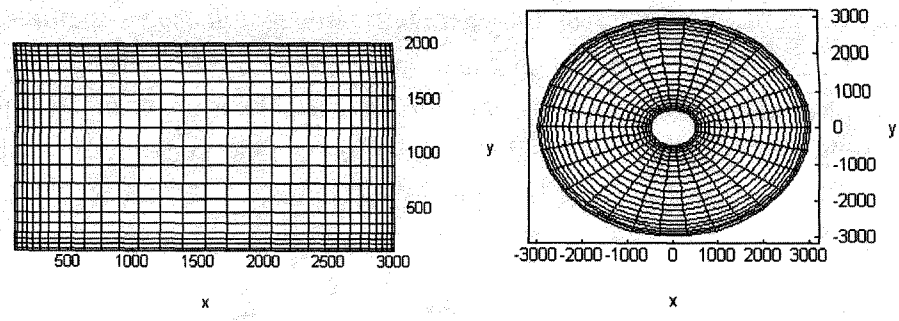

Figure 3 Non-uniform Cartesian grids with boundary clustering.

Boundary conforming structured grids can be efficiently produced by using algebraic interpolation methods. Portions of domain boundaries in physical space are associated with domain edges in computational space. Interpolation methods are utilized to generate coordinates of interior grid nodes; a two-boundary interpolation of a circle is presented in Figure 4.

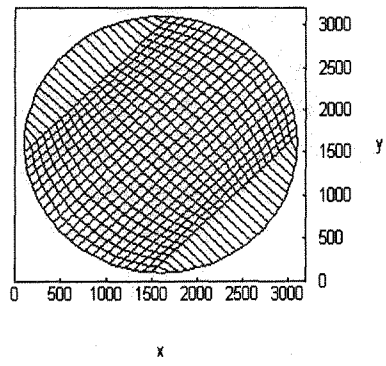

Figure 4. Boundary conforming grid generated with two-boundary interpolation.

Greater flexibility of boundary conformity can be obtained through higher order interpolation algorithms, e.g. transfinite interpolation:

$$\vec{r}_{i,j} = P^i + P^j - P^{ij}$$

$$P^i = f_i\,\vec{r}_{im,j} + (1-f_i)\vec{r}_{1,j} \quad , \quad P^j = g_j\,\vec{r}_{i,jm} + (1-g_j)\vec{r}_{i,1}$$

$$P^{ij} = f_i\,g_j\,\vec{r}_{im,jm} + f_i\,(1-g_j)\vec{r}_{im,1} + (1-f_i)\,g_j\,\vec{r}_{1,jm} + (1-f_i)(1-g_j)\vec{r}_{1,1}$$

$$f_i = \frac{i-1}{im-1} \quad , \quad g_j = \frac{j-1}{jm-1} \qquad (2)$$

The resultant grid for the same circular geometry is depicted in Figure 5. Regions around which grid nodes are concentrated and cells are distorted, correspond to the corners of the rectangle in physical space.

Porosity control on algebraic grids can be further enhanced through non-linear stretching functions or advanced mapping methods from the theory of complex variables. As an example, a simply connected arbitrary geometry polygon can be mapped onto a unit circle in the complex plane, i.e. computational space, through a series of conformal maps [6],[7].

Generation of boundary conforming curvilinear grids can also be formulated as a boundary or initial/boundary value problem (IVBP). IVBP's can be described by partial differential equation (PDE) as the governing equation over the domain and relevant initial and boundary conditions, where dependent variables are coordinates of the grid points. Since a variety of different PDE's can be used, greater control is achieved on pore sizes, clustering, continuity and orthogonality of grid lines.

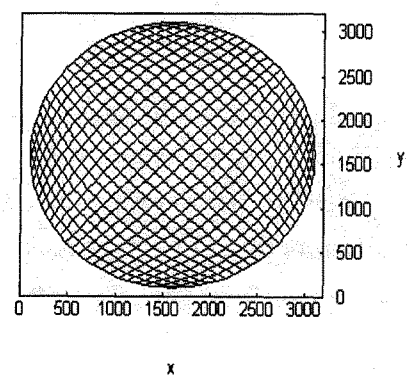

Figure 5: Boundary conforming grid generated with transfinite interpolation.

Mapping between computational and physical spaces is defined with a variable transformation, for effective construction of PDE based grid generation methods:

$$\begin{aligned} x = x(\xi,\eta) \quad &, \quad y = y(\xi,\eta) \\ \xi = \xi(x,y) \quad &, \quad \eta = \eta(x,y) \\ \begin{Bmatrix} d\xi \\ d\eta \end{Bmatrix} &= \frac{1}{(x_\xi y_\eta - x_\eta y_\xi)} \begin{bmatrix} y_\eta & -x_\eta \\ -y_\xi & x_\xi \end{bmatrix} \begin{Bmatrix} dx \\ dy \end{Bmatrix} \end{aligned} \tag{3}$$

where subscript denote partial differentiation of the dependent variable with respect to the independent variable. The most widely used PDE's are second order elliptic equations, written in the canonical form:

$$\Pi_1 \frac{\partial^2 \theta}{\partial x^2} + \Pi_2 \frac{\partial^2 \theta}{\partial y^2} + \Pi_3 \frac{\partial \theta}{\partial x} + \Pi_4 \frac{\partial \theta}{\partial y} + \Pi_5 = 0 \tag{4}$$

For grid generation, a system of elliptic PDE's can be constructed with grid coordinates as dependent variables in respective problem spaces:

$$\frac{\partial^2 \xi}{\partial x^2} + \frac{\partial^2 \xi}{\partial y^2} = P \quad , \quad \frac{\partial^2 \eta}{\partial x^2} + \frac{\partial^2 \eta}{\partial y^2} = Q \quad , \quad (\xi, \eta) = (\xi(\vec{r}), \eta(\vec{r})) \quad \vec{r} \in \Gamma_p$$

or

$$\begin{Bmatrix} L(x) \\ L(y) \end{Bmatrix} = \begin{Bmatrix} 0 \\ 0 \end{Bmatrix} \quad , \quad (x,y) = \left(x(\xi_0, \eta_0), y(\xi_0, \eta_0)\right) \quad (\xi_0, \eta_0) \in \Gamma_c \tag{5}$$

$$L \equiv A\left(\frac{\partial^2}{\partial \xi^2} + \phi \frac{\partial}{\partial \xi}\right) + 2B \frac{\partial^2}{\partial \xi \, d\eta} + C\left(\frac{\partial^2}{\partial \eta^2} + \varphi \frac{\partial}{\partial \eta}\right)$$

$$A = x_\eta^2 + y_\eta^2 \quad , \quad B = -\left(x_\xi x_\eta - y_\xi y_\eta\right) \quad , \quad C = x_\xi^2 + y_\xi^2$$

where (P,Q) are grid control parameters in physical space with their counterparts (ϕ,φ) in computational space. Since Dirichlet (constant value) type boundary conditions are specified for the BVP, the elliptic PDE's only need to be solved in the interior of the domain. The discretization of equations with central differences and employment of successive over-relaxation (SOR) iterative method, results in the following algebraic system:

$$i = 1 \ldots im, \quad j = 1 \ldots jm$$

$$x'_{i,j} = \frac{\varpi}{2(A+C)}\left[A\left(x_{i-1,j} + x_{i+1,j} + \frac{\phi}{2}\left(x_{i+1,j} - x_{i-1,j}\right)\right) + \frac{B}{2}\left(x_{i-1,j-1} - x_{i+1,j-1} - x_{i-1,j+1} + x_{i+1,j+1}\right) \right.$$
$$\left. + C\left(x_{i,j-1} + x_{i,j+!} + \frac{\varphi}{2}\left(x_{i,j+1} - x_{i,j-1}\right)\right) + (1-\varpi) x_{i,j} \right. \tag{6}$$

$$y'_{i,j} = \frac{\varpi}{2(A+C)}\left[A\left(y_{i-1,j} + y_{i+1,j} + \frac{\phi}{2}\left(y_{i+1,j} - y_{i-1,j}\right)\right) + \frac{B}{2}\left(y_{i-1,j-1} - y_{i+1,j-1} - y_{i-1,j+1} + y_{i+1,j+1}\right) \right.$$
$$\left. + C\left(y_{i,j-1} + y_{i,j+!} + \frac{\varphi}{2}\left(y_{i,j+1} - y_{i,j-1}\right)\right) + (1-\varpi) y_{i,j} \right.$$

$$A = \frac{\left(x_{i,j+1} - x_{i,j-1}\right)^2 + \left(y_{i,j+1} - y_{i,j-1}\right)^2}{4} \quad , \quad C = \frac{\left(x_{i+!,j} - x_{i-1,j}\right)^2 + \left(y_{i+1,j} - y_{i-1,j}\right)^2}{4}$$

$$B = -\frac{\left(x_{i+1,j} - x_{i-1,j}\right)\left(x_{i,j+1} - x_{i,j-1}\right) - \left(y_{i+1,j} - y_{i-1,j}\right)\left(y_{i,j+1} - y_{i,j-1}\right)}{4} \tag{7}$$

Four 51x31 grids with varying degrees of clustering were generated for a rectangular domain of which the upper boundary was replaced with the curve:

$$y = -1000\cos\left(\frac{2\pi(x-100)}{3000}\right) + 3000 \tag{8}$$

The relaxation parameter, ϖ (eq. 6), was set to 1.8 and iterations were stopped when the average cell-based residual was calculated to be less than % 0.1. The resulting grids are presented in Figure 6.

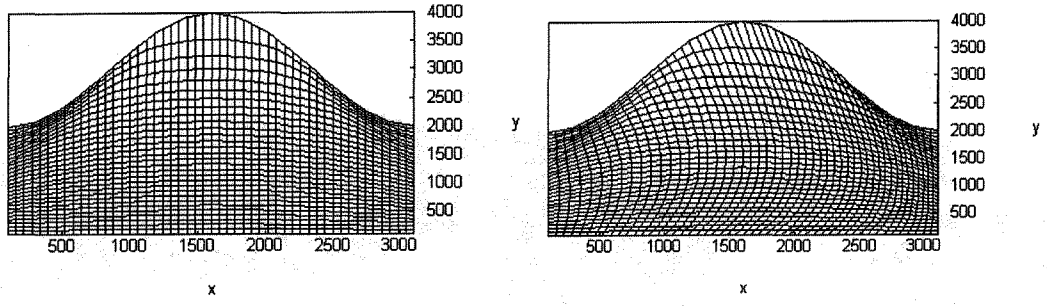

Figure 6 Curvilinear grids generated with second order elliptic PDE's: no clustering (a), clustering ($\phi = 0.03$) in ξ direction (b).

MULTI-GRID METHODS

If the solution of a computational problem requires higher grid node densities at specific locations within the domain, it is possible to generate an additional fine grid. Embedded grids, as shown in Figure 7-**a**, provide local density variations without distorting the base grid; however, the complexity of the algorithms is increased due to additional interpolation/interrogation steps. In analogy to computational physics simulations, embedded grids may provide refined porous structures.

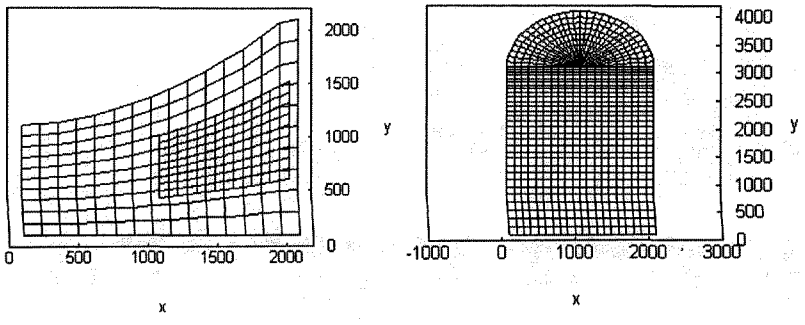

Figure 7 Sample embedded grid (a) and multi-block grid (b).

For complex geometry domains mapping of the Cartesian grid may result in severe distortion and low quality curvilinear grids, regardless of the particular method employed. Multi-block methods address grid quality by decomposing the domain into simpler geometry sub-domains, generating grids within each of them using any of the techniques described above. Multi-block grids are hybrid geometrical entities; each sub-domain is made of a structured grid but the overall grid topology is described in the context of unstructured grids (**Figure 7-b**). Multi-block grids offer increased geometric flexibility over single block structures; however, the algorithms are more complex and mostly semi-automatic.

UNSTRUCTURED GRIDS

Unstructured grids discretize the problem domain into basic geometric features that do not have implicit topology. Their connectivity is defined explicitly as part of the data-structure, in contrast to structured grids. As a result, computational methods are less efficient due to additional overhead of calculating and storing information. On the other hand, unstructured grid generation methods are geometrically more flexible and robust, since the specification of domain boundaries with closed contours (2D), or closed surfaces (3D), is sufficient for initial grid generation [8]. Triangular grids are the most widely used type of unstructured grids and can be generated with different methods:

- Mapping of a pre-triangulated mesh onto the domain using structured grid generation methods, or conversion of two-dimensional structured grids, made of quadrilaterals, into triangles.

- Delaunay triangulation, which generates triangles for a pre-specified grid node distribution optimally. Optimality is defined with the conformity of the generated triangles to equilateral triangles [9].

- Advancing front method, in which the domain boundaries define a starting front. In contrast to Delaunay triangulation, advancing front method generates interior point cloud using a set of heuristic rules [10]. Parameters and transformations within the rules can be manipulated to obtain construct tailored triangulations with relatively high computational efficiency [8].

A dual tessellation of the polygon interior can be obtained for unstructured grids by generating new points at triangle center-points (type I), or by observing distance constraints (Voronoi tessellations, type II) and constructing polygons around the old grid nodes. Interior points of Voronoi polygon V_i are closer to old grid node P_i than any other node, P_j, in the original unstructured grid. For ideal equilateral triangular grids, both constructions produce identical hexagonal dual tessellations. For arbitrary grids there are considerable differences,

where type I reflects the underlying triangulations significantly better. Figure 8 depicts a constrained Delaunay triangulation, a dual center-point tessellation and the relative layer-wise superposition for a triply connected domain, showing as these algorithms can be effectively utilized for porosity generation.

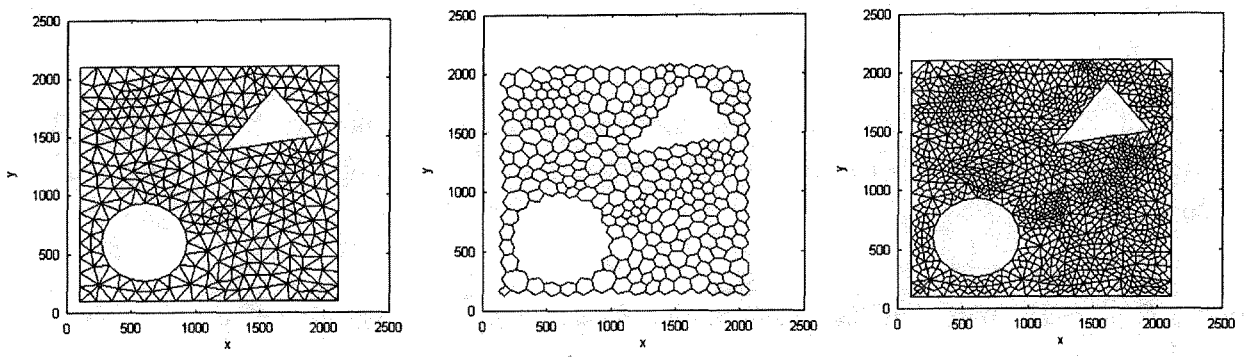

Figure 8 Triangulation (a), tessellation (b) and superposition of the two (c) on a triply connected domain.

DOMAIN DECOMPOSITION

The capabilities of individual porosity generation methods can be further amplified utilizing domain decomposition tools on layer level geometry contours. Distributions of raster angles, road widths and air-gaps can be assigned to each sub-domain by automatically modifying the properties of individual polygons in the slice (SSL) file [9]. Although domain decomposition is not as geometrically flexible as direct toolpath generation techniques described above, it can be integrated into existing process planning chain more easily.

SPACE FILLING CURVES

SFC's can be utilized as novel toolpath generation techniques in the generation of porous structures. The length of the unit steps within SFC's can be set to a value larger than width of the roads, to generate porosity. Three-dimensional porosity can be fabricated by stacking rotated or mirrored patterns of the original layer with respect to symmetry axes. See reference [9] for a more detailed description and some examples.

MULTI-MATERIAL DEPOSITION

Fused Deposition hardware (e.g. Stratasys FDM 1650) is able to deposit two different materials (modeling and support), each of which has separate delivery systems and flow

controllers. In SML language, the material for each poly-line can be specified. Hence, it is possible to specify material distributions for the porous structures inside the toolpath generation algorithms. This can be done in different ways:

- Randomly, either by assigning the material to a particular polygon through random number generators, or using center-point coordinate of the polygon and utilizing two-dimensional binary random patterns.
- With a real valued function on a plane, *f(x,y)*: the function is evaluated at the center-point of individual polygons and the material is selected based on the digitization of the calculated function.

Figure 9 shows a part that has been fabricated based on an unstructured grid of a simply connected domain and having a material distribution assigned according to a function specified as

$$f = \cos\left(\frac{x}{1000}\right)\sin\left(\frac{3y}{2000}\right).$$

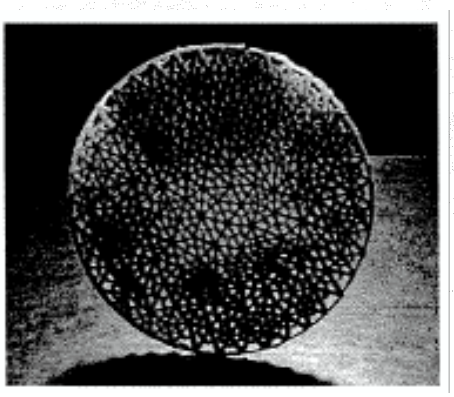

Figure 9 *Multimaterial porous structure.*

GENERATION OF POROUS STRUCTURES WIH FUSED DEPOSITION

Porous structures are described with open or closed poly-lines. A routine has been developed for the translation of poly-lines with appropriate properties into SML files [9]. In contrast to transformation based RP/SFF methods, e.g. SLA and SLS, FD necessitates the use of non-intersecting toolpaths. The minimum feature size in FD is defined by nozzle diameter and attainable road width range is currently 0.014"-0.040" for the standard 0.012" nozzles. Since one micro-step corresponds to 0.001" in *x-y* plane, the smallest controllable deposition is approximately 0.130" long. Although these bounds can be lowered using low deposition head speeds,

the minimum deposition length will not be shortened below 0.1" in the existing material delivery system, due to considerable inertia of the melt within the liquefier.

Also, due to limited communication between motion and flow controllers, straight lines, poly-lines with corners, and corners with small and large angles are not differentiated. As a result, excess material will be generated invariably at internal side of the corner, possibly closing the pores. For structures that rely on deposition of unsupported bridges, maximum pore size has been estimated as 0.150" for ABS material. However, for self-supporting structures the pore size is only bounded by the size of build domain.

SCAN-LINE DEPOSITION

Structured grids and space filling curve patterns can be effectively achieved through deposition of open-ended poly-lines. Although structured grids can also be generated using polygon deposition methods, individual grid lines within the structures are natural building blocks for scan-line deposition. Structured grids can be generated via a number of ways:

- Families of grid lines, ξ and η, can be deposed on separate layers resulting in open porous structures along the side-walls, or on the same layer, resulting in laterally closed cells and excess material accumulation at grid nodes.

- Staggered grids can be inserted into layer stacking type a, in which ξ and η lines are produced on alternating layers. Considerably reduced sagging is expected to occur in comparison to type a, due to reduced bridging lengths.

- Staggered grid ξ and η lines are produced on the same layer. Although the overall structure will have open porosity along the wall surfaces, each layer will have closed boundaries.

CONCLUSIONS

The work has presented the possibility of using Rapid Prototyping for the production of porous structures, using algorithms based on different computational approaches. Software tools have been developed and a number of porous structures has been built using a Stratasys FDM 1650 machine, showing the feasibility of all the proposed concepts. The future work will include use of polygon renumbering methods which are required for polygon-deposition of unstructured grids or their dual tessellation to shorten the deposition time as well as field adaptive unstructured grid generation techniques.

REFERENCES

1. Hague R., Dickens P., "Design of new build structures for the successful autoclaving of stereolithography models," *The Seventh International Conference on Rapid Prototyping*, pp. 192-202, March 31-April 3 1997, San Francisco, California, USA.

2. Gervasi V. R., Brandt D. A., Shaffer S. D., Lim K., "Tetracast SLA buildstyle," *The Seventh International Conference on Rapid Prototyping*, pp. 309-317, March 31-April 3 1997, San Francisco, California, USA.

3. Sun W., Lau A. C., "Knowledge-enriched CAD modeling for Solid Freeform realization of heterogeneous material structures," *The Seventh International Conference on Rapid Prototyping*, March 31 - April 3 1997, pp. 79-84, San Francisco, California, USA.

4. Thompson J. F., "Grid generation," in Minkowycz W. J., Sparrow E. M., Schneide G. E., Pletcher R. H., (eds.) *Handbook of Numerical Heat Transfer*, ISBN 0-471-83093-3, 1988.

5. Eisemann P. R., "Grid generation for fluid mechanics computations," *Annual Review of Fluid Mechanics*, vol. 17, pp. 487-522, 1985.

6. Ives, D. C., "A modern look at conformal mapping including multi-connected regions," *AIAA Journal*, vol. 14, no. 8, pp. 1006-1011, 1976.

7. Davis R. T., "Numerical methods for coordinate generation based on Schwarz-Christoffel transformations," *Proceedings of 4th AIAA Computational Fluid Dynamics Conference*, pp. 1-15, 1979

8. Löhner R., " Unstructured grid generation," in *Handbook of Fluid Dynamics and Fluid Machinery vol. 2 Experimental and Computational Fluid Dynamics*, (eds. J. A. Schetz and A. E. Fuchs), pp. 1240-1257, John Wiley & Sons, ISBN 0-471-12597-0, 1996

9. Domain Decomposition and Space Filling Curves in Toolpath Planning and Generation
M. Bertoldi, M. A. Yardimci, C. Pistor, S. I. Güçeri, Proceedings of the 1998 Solid Freeform Fabrication Symposium, The University of Texas at Austin, Austin, Texas 1998.

10. Peraire J., Vahdati M., Morgan K.,Zienkiewicz O. C, "Adaptive remeshing for compressible flow computations," *Journal of Computational Physics*, vol. 72, pp. 449-466, 1987.